Published in "Langmuir 24(15):7639–7644,2008"
which should be cited to refer to this work.

http://doc.rero.ch

Lateral Structures of Buried Interfaces in ABA-Type Triblock Copolymer Films

P. Müller-Buschbaum,*,† L. Schulz,†,‡ E. Metwalli,† J.-F. Moulin,†,§ and R. Cubitt||

Technische Universität München, Physikdepartment E13, James-Franck-Strasse 1, 85747 Garching, Germany, Université de Fribourg, Physics Department, Chemin du Musée 3, 1700 Fribourg, Switzerland, Institut für Werkstoffforschung, GKSS-Forschungszentrum Geesthacht GmbH, 21502 Geesthacht, Germany, and Institut Laue-Langevin, 6 rue Jules Horowitz, bp 156, 38042 Grenoble, France

The lateral structure of an ABA-type triblock copolymer polyparamethylstyrene-*block*-polystyrene-*block*-polyparamethylstyrene at the buried silicon substrate interface is studied as a function of different substrate surface treatments. With grazing incidence small-angle neutron scattering (GISANS), high interface sensitivity is reached. With GISANS, the orientation and degree of order of the morphology are probed. The powderlike oriented lamellar structure in the bulk orients along the surface normal in the vicinity of the substrate. A modification of the short-ranged interface potential of the substrate introduces a lateral stretching of this lamellar structure of up to 8% as compared to the bulk. The decay in stretching toward the volume structure is probed with depth profiling. It extends at least up to a distance of 51 nm from the solid surface.

1. Introduction

Self-organizing block copolymers continue to receive a great deal of attention because of their ability to form ordered nanostructures spontaneously. These nanostructures result from competition between repulsive interactions (enthalpic) and chain packing (entropic) and are sensitive to molecular design parameters, such as monomer incompatibility, molecular weight, monomer asymmetry, and composition. Of the many copolymer architectures studied, most work has concentrated on simple diblock copolymers built from immiscible monomer units (A and B). In AB diblock copolymers, a rich variety of different structures ranging from spheres to cylinders to lamellae and to a more complex bicontinuous cubic phase have been reported.[1–6]

Concerning block copolymers, the AB diblock constitutes the simplest copolymer architecture. Although the morphologies and properties of copolymers with more complex linear architectures have been investigated,[7–12] we focus here on an ABA triblock design. Similarly to AB diblock copolymers, ABA triblocks can microphase order into the classical morphologies.[13–15] In contrast to AB diblock copolymers, the mean-field phase diagrams of ABA triblock copolymers are highly asymmetric as a result of the higher entropic penalty for deforming the central B blocks so as to accommodate the two outer blocks into the A domains.[16] The principal difference between the two architectures, diblock and triblock, is the double-tethered nature of the B midblock in the triblock. Each midblock adopts either a bridged or looped conformation by depositing its ends (the block junction sites) in adjacent interphases or the same interphase, respectively. According to self-consistent field theory (SCFT)[10] and supported by experiments,[17–19] the bridging fraction lies between 0.40 and 0.45 for copolymers of modest incompatibility.

As compared to bulk morphologies, in thin films the interaction with the confining asymmetric wall (substrate and air interface) can modify the morphologies. Extensively studied for diblock copolymers, the interface energies in combination with the spatial restrictions introduced by the film thickness drive the film morphology. The preferential selectivity of one wall starts to order the copolymer film and thereby yielding an alignment of the structures parallel to this interface.[20–26] In triblock copolymer films in addition to the comparable behavior of surface-induced

* Corresponding author. Phone: +49 89 289 12451. Fax: +49 89 28912473. E-mail: muellerb@ph.tum.de.
† Technische Universität München.
‡ Universite de Fribourg.
§ Institut für Werkstoffforschung.
|| Institut Laue-Langevin.

(1) Hamley, I. W. *The Physics of Block Copolymers*; Oxford University Press: Oxford, U.K., 1998.
(2) Fredrickson, G. H. *Macromolecules* **1987**, *20*, 2535.
(3) Bates, F. S.; Fredrickson, G. H. *Annu. Rev. Phys. Chem.* **1990**, *41*, 525.
(4) Matsen, M. W.; Bates, F. S. *Macromolecules* **1996**, *29*, 1091.
(5) Förster, S.; Khandpur, A. K.; Zhao, J.; Bates, F. S.; Hamley, I. W.; Ryan, A. J.; Bras, W. *Macromolecules* **1994**, *27*, 6922.
(6) Alexandridis, P.; Olsson, P.; Lindman, B. *Langmuir* **1998**, *14*, 2627.
(7) Smith, S. D.; Spontak, R. J.; Satkowski, M. M.; Ashraf, A.; Lin, J. S. *Phys. Rev. B* **1993**, *47*, 14555.
(8) Matsushita, Y.; Mogi, Y.; Mukai, H.; Watanabe, J.; Noda, I. *Polymer* **1994**, *35*, 246.
(9) Tselikas, Y.; Hadjichristidis, N.; Lescanec, R. L.; Honeker, C. C.; Wohlgemuth, M.; Thomas, E. L. *Macromolecules* **1996**, *29*, 3390.
(10) Matsen, M. W. *J. Chem. Phys.* **1995**, *102*, 3884.
(11) Stadler, R.; Auschra, C.; Beckmann, J.; Krappe, U.; Voigt-Martin, I.; Leibler, L. *Macromolecules* **1995**, *28*, 3080.
(12) Laurer, J. H.; Bukovnik, R.; Spontak, R. J. *Macromolecules* **1996**, *29*, 5760.
(13) Laurer, J. H.; Khan, S. A.; Spontak, R. J.; Satkowski, M. M.; Grothaus, J. T.; Smith, S. D.; Lin, J. S. *Langmuir* **1999**, *15*, 7947.
(14) Wu, W.; Matyjaszewski, K.; Kowalewski, T. *Langmuir* **2005**, *21*, 1143.
(15) Matsen, M. W.; Schick, M. *Macromolecules* **1994**, *27*, 187–192.
(16) Mayes, A. M.; de la Cruz, M. O. *J. Chem. Phys.* **1991**, *95*, 4670.
(17) Watanabe, H. *Macromolecules* **1995**, *28*, 5006.
(18) Watanabe, H.; Sato, T.; Osaki, K.; Yao, M.-L.; Yamagishi, A. *Macromolecules* **1997**, *30*, 5877.
(19) Karatasos, K.; Anastasiadis, S. H.; Pakula, T.; Watanabe, H. *Macromolecules* **2000**, *33*, 523.
(20) Russell, T. P.; Coulon, G.; Deline, V. R.; Miller, D. C. *Macromolecules* **1989**, *22*, 4600.
(21) Stamm, M.; Götzelmann, A.; Giessler, K. H.; Rauch, F. *Prog. Colloid Polym. Sci.* **1993**, *91*, 101.
(22) Mansky, P.; Russell, T. P.; Hawker, C. J.; Mays, C.; Cook, D. C.; Satija, S. K. *Phys. Rev. Lett.* **1997**, *79*, 237.
(23) Torikai, N.; Noda, I.; Karim, A.; Satija, S. K.; Han, C. C.; Matsushita, Y.; Kawakatsu, T. *Macromolecules* **1997**, *30*, 2907.
(24) Müller-Buschbaum, P.; Wolkenhauer, M.; Wunnicke, O.; Cubitt, R.; Stamm, M.; Petry, W. *Langmuir* **2001**, *17*, 5567.
(25) Müller-Buschbaum, P.; Cubitt, R.; Petry, W. *Langmuir* **2003**, *19*, 7778.
(26) Busch, P.; Posselt, D.; Smilgies, D. M.; Rauscher, M.; Papadakis, C. M. *Macromolecules* **2007**, *40*, 630.

ordering,[27–31] deviations from the bulk structure were reported.[32–34]

However, despite numerous experiments that have determined the surface structure of thin copolymer films and the structure inside such films, very little information is available on the interface structure, meaning the structure of the copolymer at the substrate. This results from experimental difficulties in selectively addressing such buried interfaces. Lateral structures at surfaces are routinely probed with local imaging techniques such as atomic force microscopy (AFM) and scanning electron microscopy. In contrast, lateral structures at buried interfaces are basically inaccessible to nondestructive experimental methods. There are three examples of applied destructive methods. (I) Cross-section transmission electron microscopy which allows the measurement of the morphology and structural parameters in real space (e.g., in triblock copolymer films with high resolution).[35,36] However, the samples have to be microtomed to obtain thin sections and stained to enhance contrast. (II) Abrasive techniques such as nanotomography,[37] in which the sample volume above the buried interface is removed to use AFM. (III) Delamination of the entire film from the substrate to access the buried interface. Removal from the substrate is performed, for instance, with a razor blade[34] and can cause modifications of the interface structure as a result of the applied forces. In addition, any kinetic investigation is also prevented.

Within this investigation, we present a novel and alternative approach to probe nondestructively buried interfaces. It is based on grazing incidence small-angle neutron scattering (GISANS).[38–40] To show the possibilities of this method, we select a model system that consists of a bulky triblock copolymer film on top of a silicon substrate with a thin oxide layer (SiOx). An ABA triblock copolymer with two equal end blocks was chosen to obtain a lamellar-type microphase separation structure. The substrate surface energy was modified by four different treatments[41] covering a hydrophilic and a more hydrophobic surface type. The nanostructure due to microphase separation of the triblock copolymer is measured. We probe the differences between the structure close to the substrate surface and the bulk structure.

2. Experimental Section

Sample Preparation. The SiOx−polymer interface was prepared by spin coating (1950 rpm for 30 s). The triblock copolymer polyparamethylstyrene-*block*-polystyrene-*block*-polyparamethylstyrene, denoted P(pMS-*b*-Sd8-*b*-pMS), was prepared anionically (Polymer Standard Service; Mainz, Germany). It was spin coated out of a toluene solution onto the chemically modified SiOx surface. Storage under a toluene vapor atmosphere (pressure $p = 0.8p_0$, temperature 296 K) was applied to allow the structure of the triblock copolymer to come to equilibrium. After 14 h of storage, the sample were quenched in ambient air and examined. The nearly symmetric P(pMS-*b*-Sd8-*b*-pMS) had a fully deuterated polystyrene middle block (M_w = 140 000 g/mol), two equally sized protonated polyparamethylstyrene blocks (each of M_w = 70 000 g/mol), and a total molecular weight of M_w = 280 000 g/mol (narrow molecular weight distribution of $M_w/M_N = 1.1$). The degree of polymerization of the PSd block compared to the total chain was $f_{PSd} = N_{PSd} = 0.51$. Thus, the internal nanostructure resulting from microphase separation in bulklike P(pMS-*b*-Sd8-*b*-pMS) films is a randomly oriented lamellae with a powderlike orientation of the lamellar domains.

A modification of the short-ranged interface potential of the silicon substrate was introduced by applying four different surface treatments.[41] Immediately before spin coating, the Si substrate was treated with an acid bath and a basic bath, polydimethylsiloxane (PDMS) grains were deposited on the surface, and a polystyrene (PS) layer was grafted onto the substrate. The acid bath consisted of 100 mL of 80% H_2SO_4, 35 mL of H_2O_2, and 15 mL of deionized water. After 15 min at 80 °C in the acid bath, the substrates were taken out, rinsed in deionized water, and dried with compressed nitrogen. For the basic bath, the samples were placed in dichloromethane in an ultrasonic bath for 5 min and rinsed with Millipore water shortly afterwards. Then the substrates were kept for 2 h in an oxidation bath at 75 °C consisting of 1400 mL of Millipore water, 120 mL of H_2O_2, and 120 mL of NH_3 to clean all organic traces off of the surface. Thereafter, the samples were stored in Millipore water. Directly before spin coating, the substrates were rinsed with Millipore water at least five times to remove possible traces of the oxidation bath and dried with compressed nitrogen as well. The acid and basic treatments resulted in a thin silicon oxide layer (thickness 1 nm) covering the Si surface. PDMS was deposited from a toluene solution on the SiOx. The size of the PDMS grains was small as compared to the characteristic lengths of the triblock copolymer (i.e., the lamellar spacing). In terms of rms surface roughness, the deposition of the PDMS grains caused an increase from 0.5 to 1.2 nm. Typically, the height of the grains was <1 nm, and the diameter was in the order of 3 nm. The PS layer was grafted via a grafting-to procedure by annealing a spin-coated layer of the corresponding carboxy-terminated PS above the glass-transition temperature[42] and removal of the excess amount. A thickness of 5 nm was installed by controlling the annealing time. With respect to the static water contact angle, these four different treatments result in a range of $\Theta = 0$ (base) to 20 (acid) to 35 (PDMS grains) to 91° (PS brush).

Grazing Incidence Small-Angle Neutron Scattering Experiments. GISANS measurements were performed at the D22 beamline at the ILL neutron reactor (Grenoble, France) at a wavelength of 0.6 nm (wavelength selector $\Delta\lambda/\lambda = 10\%$), a sample−detector distance of 14.4 m, and a collimation of 17.6 m. The measurements were performed at four angles of incidence (0.075, 0.162, 0.213, and 0.727°). The error in the angle of incidence was 0.008°. It was determined by the accuracy of the alignment, which was given by the half-size of a pixel of the detector at the given distance. The GISANS information in the recorded 2D intensity map was extracted from slices parallel to the sample surface at the critical angle.[38,39] Statistics of these slices were improved by integrating the intensity over the two neighboring detector lines corresponding to $\Delta q_z = \pm 2.33 \times 10^{-2}$ nm^{-1}. The experimental resolution was 3×10^{-3} nm^{-1}.

Following the sample geometry that is successfully used in neutron reflectometry,[43–45] the neutron beam impinges not from the polymer film surface but through the silicon (Si) substrate (Figure 1). Whereas

(27) Sakurai, S.; Aida, S.; Okamoto, S.; Ono, T.; Imaizumi, K.; Nomura, S. *Macromolecules* **2001**, *34*, 3672.
(28) Finne, A.; Andronova, N.; Albertsson, A. C. *Biomacromolecules* **2003**, *4*, 1451.
(29) Shin, D.; Shin, K.; Aamer, K. A.; Tew, G. N.; Russell, T. P.; Lee, J. H.; Jho, J. Y. *Macromolecules* **2005**, *38*, 104.
(30) Wu, W.; Huang, J.; Jia, S.; Kowalewski, T.; Matyjaszewski, K.; Pakula, T.; Gitsas, A.; Floudas, G. *Langmuir* **2005**, *21*, 9721.
(31) Müller-Buschbaum, P.; Maurer, E.; Bauer, E.; Cubitt, R. *Langmuir* **2006**, *22*, 9295.
(32) Rehse, N.; Knoll, A.; Konrad, M.; Magerle, R.; Krausch, G. *Phys. Rev. Lett.* **2001**, *87*, 035505.
(33) Krausch, G.; Magerle, R. *Adv. Mater.* **2002**, *14*, 1579.
(34) Epps, T. H., III; DeLongchamp, D. M.; Fasolka, M. J.; Fischer, D. A.; Jablonski, E. L. *Langmuir* **2007**, *23*, 3355.
(35) Xu, T.; Hawker, C. J.; Russell, T. P. *Macromolecules* **2003**, *36*, 6178.
(36) Sivaniah, E.; Hayashi, Y.; Iino, M.; Hashimoto, T.; Fukunaga, K. *Macromolecules* **2003**, *36*, 5894.
(37) Magerle, R. *Phys. Rev. Lett.* **2000**, *85*, 2749.
(38) Müller-Buschbaum, P.; Gutmann, J. S.; Stamm, M. *Phys. Chem. Chem. Phys.* **1999**, *1*, 3857.
(39) Müller-Buschbaum, P.; Gutmann, J. S.; Cubitt, R.; Stamm, M. *Colloid Polym. Sci.* **1999**, *277*, 1193.
(40) Wolff, M.; Magerl, A.; Zabel, H. *Eur. Phys. J. E* **2005**, *16*, 141.
(41) Müller-Buschbaum, P. *Eur. Phys. J. E* **2003**, *12*, 443.
(42) Ionov, L.; Sidorenko, A.; Stamm, M.; Minko, S.; Zdyrko, B.; Klep, V.; Luzinov, I. *Macromolecules* **2004**, *37*, 7421.
(43) Rennie, A. R.; Lee, E. M.; Simister, E. A.; Thomas, R. K. *Langmuir* **1990**, *6*, 1031.
(44) Lu, J. R.; Thomas, R. K. *J. Chem. Soc., Faraday Trans.* **1998**, *94*, 995.
(45) Gutberlet, T.; Klosgen, B.; Krastey, R.; Steitz, R. *Adv. Eng. Mater.* **2004**, *6*, 832.

http://doc.rero.ch

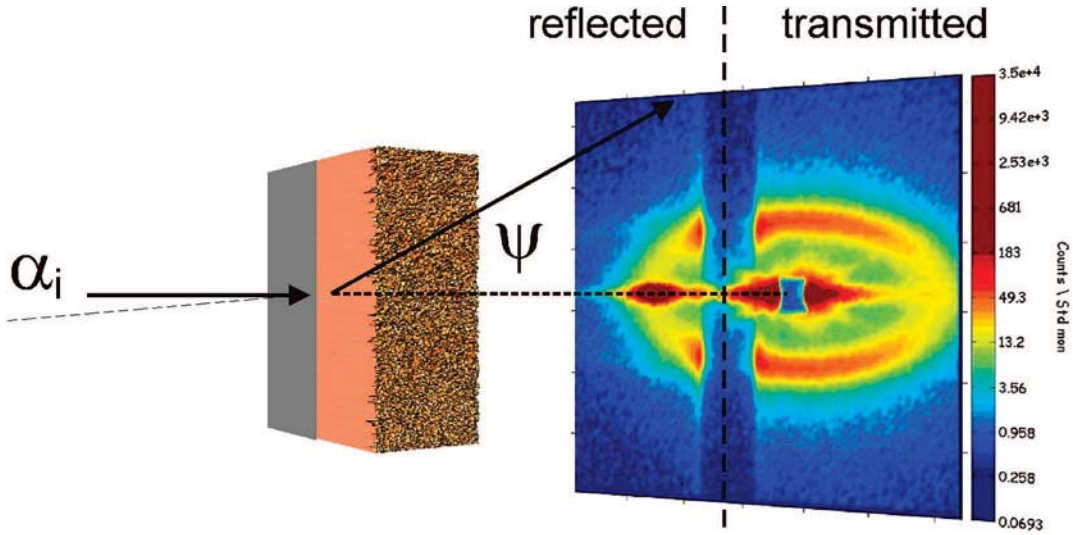

Figure 1. Schematic picture of the experimental setup used in the GISANS measurements. The neutron beam impinges through the silicon substrate. The angle of incidence with respect to the sample horizon is denoted α_i, the exit angle α_f, and the out-of-plane angle ψ. With the 2D detector, the reflected and transmitted signal is probed.

http://doc.rero.ch

specular neutron reflectivity is limited to the detection of the density profile and has no access to lateral structures, GISANS probes a lateral structure in the length-scale regime from molecular dimensions on the nanometer level up to a few micrometers. So far, GISANS experiments were limited to the scattering geometry with the neutron beam impinging from the top of the polymer film. Becauseof the higher scattering-length density (SLD) for the neutron in deuterated polymer compared to Si, total reflection at the SiOx−polymer interface can occur, which is the key to becoming interface-sensitive.[46–48] In contrast, in X-ray experiments, because of the missing contrast enhancement by deuteration, polymer materials typically have a smaller refractive index than does the Si substrate, and total reflection is possible only if the X-ray beam comes from the polymer side, such that one can limit penetration into the substrate but not into the film. Therefore, the more standard technique of grazing incidence small-angle X-ray scattering (GISAXS) cannot be applied. Moreover, contrary to X-rays the absorption for neutrons in the Si substrate is small, and the signal not strongly attenuated by passing through the substrate.

3. Results and Discussion

Volume Structure. The polymer−polymer interaction parameter of dPS and PpMS in a blend is $\chi = A + B/T$ with $A = -0.011 \pm 0.002$ and $B = 6.8 \pm 1$ K, which yields $\chi N \approx 15$.[49] In the block copolymer, the polymer−polymer interaction parameter typically is larger than in the blend, which gives rise to an even larger value of χN, and thus the strong segregation regime is addressed. To probe the bulk structure, GISANS experiments were performed at an angle of incidence above the effective critical angle of the triblock copolymer films in contact with the silicon substrate ($\alpha_i > \alpha_c$). The extracted slices parallel to the sample surface are shown in Figure 2a. The strong intensity maxima in the curves are located at the same q_y position, independent of the surface treatment. The solid lines are fits in the framework of the distorted wave Born approximation (DWBA). In the DWBA, the differential cross section can be approximated by diffuse scattering from one rough interface[50,51]

$$\frac{d\sigma}{d\Omega} = A(Nb)^2|T_i|^2|T_f|^2F(\vec{q})$$

because of the large film thickness and the chosen geometry, where A is the illuminated surface area, Nb is the coherent SLD jump at the Si−polymer interface, $T_{i,f}$ is the Fresnel transmission functions, and $F(q)$ is the diffuse scattering factor. Because α_i and α_f are fixed in GISANS, the Fresnel transmission functions $T_{i,f}$ act only as overall scaling factors, and the diffuse scattering factor $F(q)$ is directly detected. For N identical centrosymmetrical objects with a random orientation, the diffuse scattering factor can be approximated to depend on the form factor of the individual objects $P(q)$ and on the structure factor $S(q)$:

$$F(\vec{q}) \approx NP(\vec{q})\, S(\vec{q})$$

A mathematical description of the form factor depends on the type of object, and the structure factor directly yields the most prominent in-plane length. In the model used, $F(q)$ takes the lamellar structure with a Lorentzian-distributed length, a form factor with a Lorentzian-shaped polydispersity, and the resolution function of the experimental setup into account. The strong maximum probed in this investigation is the first-order Bragg peak and corresponds to the bulk lamellar spacing $L_{bulk} = 48 \pm 3$ nm The second-order Bragg peak is only shoulderlike as expected for a symmetric lamellar system (with A and B of equal size) and is due to the disorder in the system. Hence, the microphase separation structure in the bulklike film is not affected by the surface treatment and is equal to the standard bulk structure of P(pMS-*b*-Sd8-*b*-pMS).[31]

Interface Structure. Upon variation of the angle of incidence in the GISANS experiments, interface sensitivity was achieved. The critical angle of incidence for the investigated system (silicon/copolymer interface) is $\alpha_c = 0.24°$ (calculated from $Nb = 1.505 \times 10^{-6}$ Å^{-2}),[52] and the total film thickness is 882 nm. At angles of incidence smaller than the critical angle, the transmitted wave is exponentially damped into the less dense medium, and the

(46) Sinha S. K. In *Neutron Scattering in Materials Science*; Neumann, D. A., Russell, T. P., Wuensch, B. J., Eds.;MRS Symposia Proceedings No. 376; Materials Research Society: Pittsburgh, PA, 1995; p 175.
(47) Schreyer, A.; Ankner, J. F.; Zeidler, Th.; Zabel, H.; Schäfer, M.; Wolf, J. A.; Grünberg, P.; Majkrzak, Z. F. *Phys. Rev. B* **1995**, *52*, 16066.
(48) te Velthuis, S. G. E.; Jiang, J. S.; Bader, S. D.; Felcher, G. P. *Phys. Rev. Lett.* **2002**, *89*, 127203.
(49) Schnell, R.; Stamm, M. *Physica B* **1997**, *234−236*, 247.
(50) Pynn, R. *Phys. Rev. B* **1992**, *45*, 602.
(51) Leroy, F.; Lazzari, R.; Renaud, G. *Surf. Sci.* **2007**, *601*, 1915.
(52) Using the NIST tool at http://www.ncnr.nist.gov/resources/sldcalc.html.

penetration of the beam into the sample is limited. As well known from grazing incidence diffraction (GID),[53] to determine the depth from where the observed scattering originates, both the selected incident and exit angle $\alpha_{i,f}$ have to be taken into account. For both grazing angles and the difference in the SLDs, *Nb* defines the smallest accessible scattering depth of the signal. With

$$D = \frac{\lambda}{\sqrt{2}\pi(l_i + l_f)}$$

and

$$l_{i,f} = \left[(\alpha_c^2 - \alpha_{i,f}^2) + \sqrt{(\alpha_{i,f}^2 - \alpha_c^2)^2 + 4\beta^2}\right]^{1/2}$$

the scattering depth D of the neutrons is calculated using the relative critical angle

$$\alpha_c = \lambda\sqrt{\frac{Nb}{\pi}}$$

and absorption

$$\beta = \frac{\lambda\mu_n}{4\pi}$$

The GISANS signals were probed over the characteristic depth, D, into the polymer. (D resembles the distance from the Si substrate.) Figure 2b shows the corresponding line cuts for the smallest angle of incidence, thereby probing the structure closest to the Si substrate. Irrespective of the surface treatment, a peak is visible, indicating the presence of a structure oriented along the surface normal, which we identify to be a perpendicular lamella. However, in more detail, the peak intensity, the peak width, and the q_y position depend on the substrate treatment.

To deduce the extension of order inside the polymer films for the different substrate interfaces as a function of the distance from the interface, in a series of GISANS experiments different angles of incidence were chosen: α_i/α_c= 0.313, 0.675, 0.888, and 3.029. Three angles were selected that were smaller than the critical angle of the triblock copolymer in contact with the Si substrate, and one angle was selected that was larger. This results in ratios of q_z/q_c= 0.656, 0.838, 0.944, and 2.015. Instead of full 2D intensities, we again restrict the presentation to selected cuts. The resulting slices parallel to the sample surface are displayed in Figure 2c for the base-cleaned sample and in Figure 2d for the PS brush. The former represents the unstretched-chain and the latter represents the stretched-chain scenario (Figure 3). At an angle of incidence above the critical angle, the powder-like-oriented nanostructure of the polymer gives rise to the intensity maxima. At angle of incidence below the critical angle, the probed polymer volume was restricted to the part near the interface (scattering depths of D = 24, 31, and 51 nm). The larger the value of D, the more in-depth information about the structure is incorporated into the scattering signal. The result is in fact an average structure weighted by an exponential of characteristic depth D into the surface. The restricted probed volume explains the reduced peak intensity. As for the bulk at the interface, mainly the first-order Bragg peak dominates the scattering. The presence of intensity maxima in these slices parallel to the sample surface can be explained only by the existence of a well-ordered lamellar structure in the region close to the polymer−SiOx interface given by the scattering depth. This lamellar structure is oriented perpendicular with respect to the substrate surface. It caps the

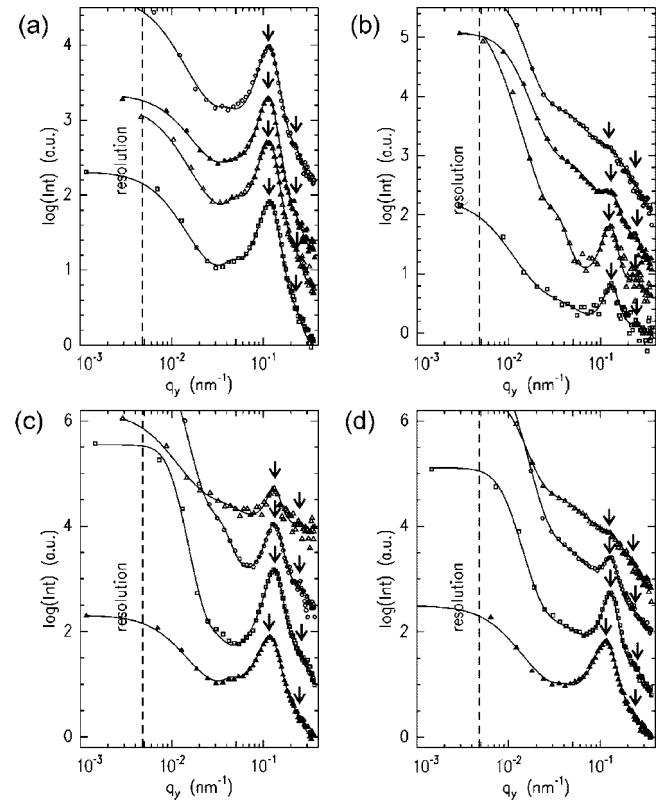

Figure 2. Slices parallel to the sample surface at the critical angle α_c of the polymer against Si (shifted for clarity along the y axis) (a) for an angle of incidence of $\alpha_i > \alpha_c$; (b) for an angle of incidence of α_i/α_c = 0.313, both for the four different surface treatments (from bottom to top: base-cleaned, PDMS grains, acid-cleaned, and PS brush); (c) for the base-cleaned; and (d) for the PS brush surface sample, both for different angles of incidence (from bottom to top: α_i/α_c= 3.029, 0.888, 0.675, and 0.313). Bragg positions are indicated with small arrows, and the dashed line marks the resolution with respect to large lateral structures.

powder-like-oriented bulk structure at the buried SiOx−polymer interface.

Figure 4 displays the increase in the lamellar spacing close to the SiOx substrate measured for the surface treatments. For the acid-cleaned sample, the PDMS grains and the PS brush at a larger distance from the SiOx surface, the increase decays before the bulk value is reached. With increasing distance from the substrate, chains are less stretched because the enthalpic contribution from the substrate is reduced. However, the maximum stretching and the decay in chain stretching depend on the surface treatment. Figure 5 shows the dependence of the peak width as a function of distance from the substrate interface. It resembles the degree of order. Irrespective of the substrate treatment in the interface near region, the order is increased ($\omega_0/\omega_{bulk} < 1$), which is due to the presence of the perpendicular lamellar instead of the random orientation of the lamella. The curves shown in Figures 4 and 5 do not represent the real functions but are averages showing a general trend of structural change toward the interface.

In Figure 3, possible scenarios of the morphology at the substrate interface are pictured. Figure 3c,d illustrates the development of an order parallel to the substrate surface, which can be excluded from the presence of Bragg peaks in the slices parallel to the sample surface. Whereas in diblock copolymer films the selectivity of the substrate to one block or the other definitively introduces this lamellar order parallel to the sub-

(53) Dosch, H.; Batterman, B. W.; Wack, D. C. *Phys. Rev. Lett.* **1986**, *56*, 1144.

http://doc.rero.ch

http://doc.rero.ch

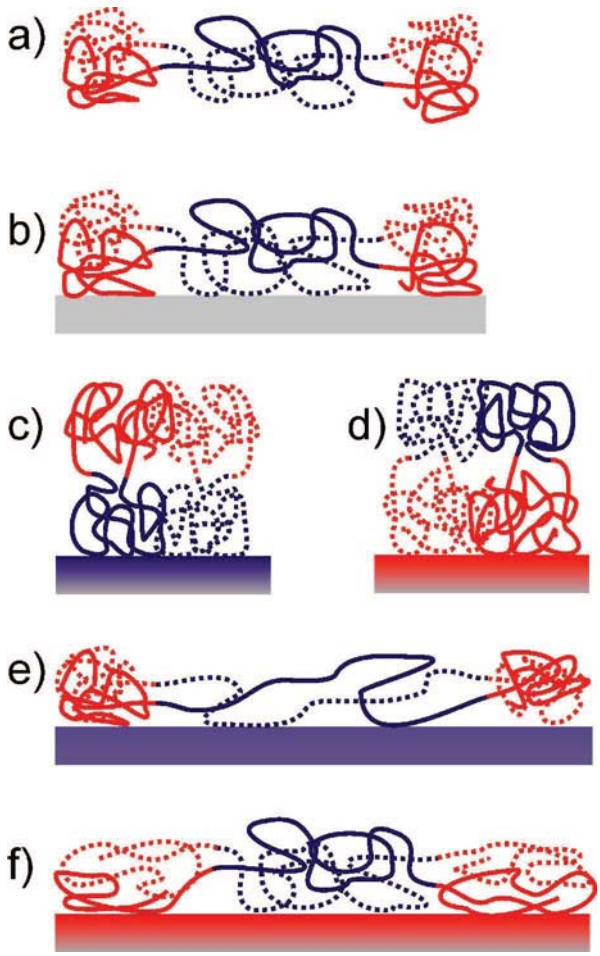

Figure 3. Possible scenarios arising with an ABA triblock copolymer chain (a) in the bulk volume, (b) in contact with a neutral wall, (c, e) in contact with a midblock (B-type) selective wall, and (d, f) in contact with an end-block (A-type) selective wall. In each sketch, two chains are shown, one with a solid and one with a dashed line.

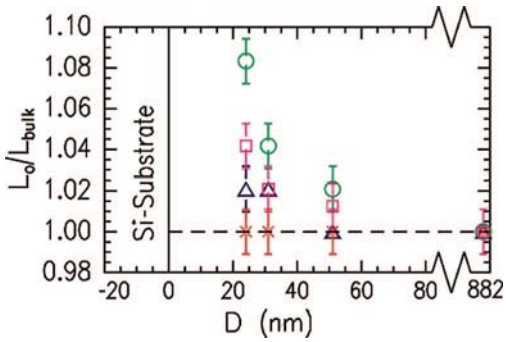

Figure 4. Lamellar spacing L_o normalized by the bulk lamellar spacing L_{bulk} probed as a function of the scattering depth D of the signal (i.e., the depth over which the signal is probed with the evanescent wave) for the sample after acid cleaning (triangles) and base cleaning (crosses), with deposited PDMS grains (squares) and the PS brush surface (spheres). The dashed line shows the bulk lamellar spacing. The SiOx substrate is indicated.

strate,[54,55] for the investigated triblock copolymer the situation is different. The reason is the entropic penalty in deforming the central blocks so as to accommodate the two outer blocks into

(54) Menelle, A.; Russell, T. P.; Anastasiadis, S. H.; Satija, S. K.; Majkrzak, C. F. *Phys. Rev. Lett.* **1992**, *68*, 67.
(55) Mansky, P.; Russell, T. P.; Hawker, C. J.; Mays, J.; Cook, D. C.; Satija, S. K. *Phys. Rev. Lett.* **1997**, *79*, 237.

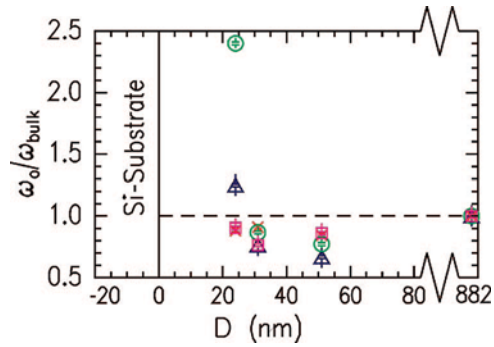

Figure 5. Full width at half-maximum ω_0 of the first-order Bragg peak of the interface signal normalized with the bulk value ω_{bulk} as a function of the scattering depth D for the sample after acid cleaning (triangles) and base cleaning (crosses), with deposited PDMS grains (squares) and the PS brush surface (spheres). The dashed line shows the bulk full width at half-maximum. The SiOx substrate is indicated.

the domains with a morphology that differs from that of a perpendicular lamellae.[30] Therefore, the bulk phase diagram is dominated by the lamellar phase, and changes in the surface energy do not stabilize into new morphologies (such as cylinders or spheres) or cause a transition of the lamellar orientation (perpendicular to parallel). Instead, the lamellae is oriented perpendicular to the substrate interface, and the type of interface determines whether the chains stay unstretched (Figure 3b) or get stretched by stretching the midblock (Figure 3e) or the end blocks (Figure 3f).

Neutral Wall. In general, the alignment of block copolymer microdomains depends on the segmental interaction between two blocks and the difference in the interfacial energies of each block with the substrate. By applying alternative surface treatments, the short-ranged interface potential is altered. In the case in which the substrate surface is neutral (i.e., where the interfacial interactions of both blocks with the substrate are the same), there is no preferential wetting, and the chain remains unstretched (Figure 3b). The microphase separation structure is oriented normal to the substrate interface. This orientation persists a few periods from the interface before a randomization of the microdomain orientation occurs.

For the base cleaning irrespective of the scattering depth the lamellar orientation remains unchanged as compared to the bulk. Because the base cleaning results in a hydrophilic substrate surface (water contact angle of $\Theta = 0°$) that is unfavorable for both blocks, the obtained surface is nonpreferential for both blocks. Because of the large film thickness, dewetting is suppressed, and both blocks stay equally at the interface. The oriented nanostructure exists at least up to a distance of 51 nm from the Si surface. The degree of order at the interface and in the near-interface region is higher as compared to that in the random bulk. Thus, GISANS with depth resolution provides a measure of the range of ordering in the surface field.

For the surface with deposited PDMS grains, after acid cleaning and on the PS brush the behavior is more complicated:

Midblock Selective Wall. In cases of a preferential substrate interaction, one block has a much lower interfacial energy with respect to the substrate. Typically, in many recent experiments the interfacial energy was controlled precisely by anchoring a random copolymer brush to the substrate.[56] Within this work, we selected a PS brush that will favor the presence of the PS block close to the substrate, so the substrate favors increased contact of the midblock, which results in stretching of the

(56) Xu, T.; Hawker, C. J.; Russell, T. P. *Macromolecules* **2005**, *38*, 2802.

midblock. This causes an increase in the observed lamellar spacing of 8% (PS brush) as compared to the bulk value. At the interface, it is accompanied by an increase in disorder, whereas in the near-interface region the order is improved by alignment as compared to the bulk. These findings might be interpreted with more defects building in by the strongest stretching of the midblock, whereas moderate stretching allows for improved ordering.

End-Block-Selective Wall. The acid treatment and the PDMS-covered surface present less hydrophilic surfaces (water contact angles of $\Theta = 20$ and 35°). Both will favor wetting with the block with the lower surface tension (γ(PpMS)/γ(PS) = 0.86), and the PpMS block is expected to be in close contact with the surface. Because of the finite smallest angle of incidence that was realized in the experiment ($\alpha_i/\alpha_c = 0.313$) and the given contrast in the SLD of the Si substrate and the triblock copolymer film, the scattering depth cannot reach zero. As a consequence, we have no direct access with GISANS to the layer directly in contact with the surface. However, we can exclude the build up of a parallel orientation that extends into the film, because (as shown before) at the closest accessible distance to the SiOx−polymer interface ($D = 24$ nm) a lateral structure is detected. Thus, the investigated triblock copolymer behaves differently from diblock copolymers,[54,55] which favor parallel orientation with respect to the substrate. Therefore, the substrate favors increased contact of the end blocks, which results in a stretching of the end blocks (Figure 3f). Instead of introducing a parallel orientation that extends into the film, the change in the surface field causes a slight increase in the lamellar spacing by 2 (acid-clean) and 4% (PDMS grains) in comparison with the bulk. Again, for both in the near-interface region the alignment effect causes an increase in order. However, at the interface the degree of order depends very much on the applied treatment, and for the acid-cleaned and PDMS grains an opposite behavior is found.

4. Conclusions

We have demonstrated the potential of GISANS to access lateral structures at buried interfaces and to obtain a depth resolution in the model system of microphase separation-induced nanostructures in triblock copolymer films. For the investigated P(pMS-*b*-Sd8-*b*-pMS) films irrespective of the applied substrate surface treatment, a perpendicular alignment of the lamellar at the interface was observed, so bending of the midblock is avoided in any case. In detail, the bulk conformational properties of polymer chains are modified in contact with the interface as a result of competition between the loss of entropy at the interface and the gain of internal energy.

In general, GISANS enables the detection of small changes in characteristic lateral lengths such as the lamellar spacing of the copolymer. Of course, the technique is not at all limited to copolymer films or soft matter systems. The only necessary conditions are the transparency of the substrate for the neutron beam and a jump in the SLD at the substrate−film interface that allows for total reflection (i.e., the SLD of the film is larger than that of the substrate). Thus, a large SLD of the film enables us to probe structures closer to the substrate−film interface. Experimentally, this requires high neutron beam collimation and access to very small angles $\alpha_{i,f}$. The depth profiling requires a high precision in the variation of the angle of incidence.

Acknowledgment. The preparation of the PS brush surfaces was performed by P. Uhlmann in the group of M. Stamm at the Leibniz Institute of Polymer Research Dresden. This work was financially supported by DFG in the priority program SPP1164 (grant MU1487/2).

http://doc.rero.ch